ACS OMEGA

http://pubs.acs.org/journal/acsodf

Article

Solution-Processed All-inorganic Planar Heterojunction Solar Cells by Employing In Situ Grown Interfacial Layer with Dual Functions: Complementary Absorption and Selective Extraction of Photogenerated Holes

Wangwei Chen, Wenbo Cao, Rong Liu, Chao Dong,* Zhiyang Wan, Junwei Chen, Getinet Y. Ashebir, and Mingtai Wang*

Cite This: *ACS Omega* 2021, 6, 6973−6980

Read Online

ACCESS | Metrics & More | Article Recommendations | Supporting Information

ABSTRACT: Photovoltaic conversion of renewable solar energy into electricity for sustainable energy production requires efficient, stable, and low-cost solar cells. Developing solution-processed all-inorganic solar cells is a practical scenario in virtue of the high charge mobility and good stability of inorganic semiconductors. Here, for the first time, we present a solution-processed all-inorganic planar heterojunction solar cell based on the nanoparticle film of copper indium sulfide ($CuInS_2$) by using an antimony trisulfide (Sb_2S_3) nanoparticle film as an interfacial layer between the $CuInS_2$ photon-harvesting layer and cathode. All of the component layers in the solar cell are in a superstrate architecture and sequentially in situ grown on a transparent conducting glass acting as anode by solution-processing methods. The dependences of device performance on the thickness of Sb_2S_3 film and the reduction of hole-trapping centers in the Sb_2S_3 film by thioacetamide treatment are investigated. The optimized all-inorganic device exhibits the best power conversion efficiency of 4.85% under AM 1.5G illumination and an excellent thermal stability. It is found that the Sb_2S_3 interfacial layer sandwiched between the $CuInS_2$ photon-harvesting layer and counter-electrode has dual functions, that is, to provide complementary absorption after $CuInS_2$ attenuation and to act as an effective hole-transporting layer to selectively extract photogenerated holes for effective charge collection efficiency.

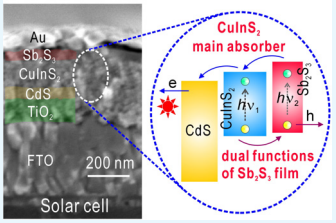

1. INTRODUCTION

Renewable solar energy is a vital source for sustainable energy production. Photovoltaic conversion of solar energy into electricity requires efficient, stable, and low-cost solar cells, which is inspiring the research on solution-processable materials systems for such photovoltaic devices. The ternary compound $CuInS_2$ is one of the promising light-harvesting materials for efficient solar cells due to its high stability, suitable band gap ($E_g \sim 1.6$ eV), and large absorption coefficient ($\alpha \sim 10^5$ cm^{-1}) in the visible range.[1−4] The power conversion efficiency (η) of $CuInS_2$-based single-junction solar cells is theoretically expected to reach 30−32% according to Shockley−Queisser limit.[5] Planar heterojunction solar cells are of great interest because of the easily prepared superstrate configuration therein. Although a suitable hole-transporting material (HTM) layer for selective extraction of photogenerated holes is indispensable for efficient solar cells based on inorganic absorbers,[6] almost no HTM layer was normally used between the $CuInS_2$ absorbing film and collection electrode in $CuInS_2$-based planar heterojunction solar cells[7−11] resulting in the efficiency of only 3.0−4.0% in most ITO(FTO)/$CuInS_2$/CdS/Al planar heterojunction devices, for example.[7,8] Previously, we developed a solution method to prepare a high-quality $CuInS_2$ nanoparticle layer on a TiO_2/CdS film and achieved an efficiency of 6.31% under AM 1.5G illumination (100 mW/cm^2) in the planar heterojunction solar cells of an ITO/TiO_2/CdS/$CuInS_2$/Spiro-OMeTAD/Au structure with Spiro-OMeTAD as an organic HTM.[12] However, Spiro-OMeTAD is not a perfect HTM for future practical applications subjected to its high cost and low long-term stability.[13] The demands for the low-cost and stable HTM in efficient solar cells have encouraged the pursuit of inorganic HTMs, such as NiO_x and CuSCN for Sb_2S_3 and perovskite solar cells[13−17] and CuO_x for perovskite and organic solar cells.[18,19]

Sb_2S_3, a nontoxic and earth-abundant material, is a promising light absorber for solar cells due to its high stability, suitable band gap of 1.7−1.8 eV, and high light absorption coefficient (>10^5 cm^{-1}) in the visible region;[20,21] in particular, it has rather high mobility (μ) of holes ($\mu_h \approx 2.6$ cm^2 V^{-1} s^{-1})[15] and electrons ($\mu_e \approx 10$ cm^2 V^{-1} s^{-1}).[22] In this paper, for the first time, we use an in situ grown Sb_2S_3 film as the interfacial layer between the $CuInS_2$ film and collection

Received: December 22, 2020
Accepted: February 17, 2021
Published: March 2, 2021

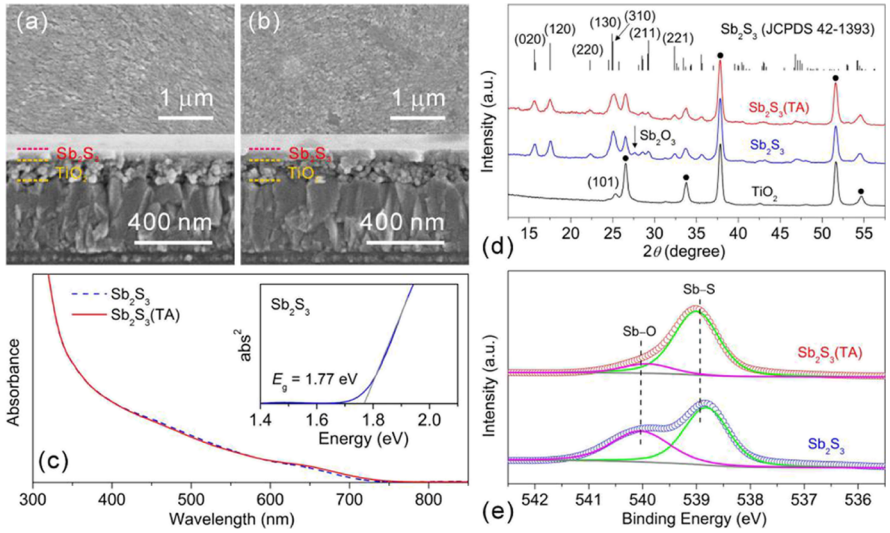

Figure 1. (a,b) SEM images (above: bird's eye view; below: cross-sectional view), (c) absorption spectra, (d) XRD pattern, and (e) XPS Sb 3d spectra of the Sb_2S_3 (a) and Sb_2S_3(TA) (b) films on FTO/TiO_2 substrates. The inset in (c) shows that the E_g of the Sb_2S_3 layer is about 1.77 eV, evaluated by the direct band gap method, that is, plotting the squared absorbance (abs^2) versus energy (eV) and extrapolating to zero. On plot (d), the XRD pattern of TiO_2 film on FTO is used for comparison and the symbol ● indicates the XRD peak of FTO substrate.

electrode and obtain a solution-processed all-inorganic $CuInS_2$-based planar heterojunction solar cell configurated as FTO/TiO_2/CdS/$CuInS_2$/Sb_2S_3/Au. We find that the Sb_2S_3 interfacial layer acts both as the complementary absorber after $CuInS_2$ attenuation and as an effective HTM layer for improving the charge collection efficiency, and thioacetamide (TA) treatment of the Sb_2S_3 film further improves device performance by enhancing the interfacial hole extraction efficiency.

2. RESULTS AND DISCUSSION

2.1. In Situ Growth of Sb_2S_3 Film. In order to avoid the interference of the underlying CdS/$CuInS_2$ layer and get a simple characterization, the in situ grown Sb_2S_3 film was investigated by using FTO/TiO_2 substrate. Scanning electron microscopy (SEM) images show that the Sb_2S_3 film and the Sb_2S_3 film treated by TA (sampled as Sb_2S_3(TA) film) have a uniform thickness of ca. 50 nm over the TiO_2 layer (ca. 120 nm), and the TiO_2/Sb_2S_3 interface is clearly observed (Figure 1a,b). In particular, the morphology and thickness of Sb_2S_3 film before and after the TA treatment are not evidently changed, indicating that TA treatment imposes almost no influence on the morphology and thickness of the Sb_2S_3 film. Absorption spectra (Figure 1c) show that the Sb_2S_3 and Sb_2S_3(TA) films have identical absorption features, with an optical band gap (E_g) of 1.77 eV.

Both Sb_2S_3 and Sb_2S_3(TA) films exhibit the X-ray diffraction (XRD) peaks at around 15.61, 17.50, 22.30, 25.11, 29.25, and 32.36° (Figure 1d), matching well with the (220), (120), (220), (130)/(310), (211), and (221) crystal planes of Sb_2S_3 (stibnite) (JCPDS card 42-1393). However, the peak at 27.64° due to the Sb_2O_3 phase[23,24] is much weaker for Sb_2S_3(TA) film than for the Sb_2S_3 one. The average size (D) of the Sb_2S_3 nanocrystals of the two samples is calculated to be ∼16 nm according to Scherrer formula $D = K\lambda(B\cos\theta)^{-1}$ where K is a constant (0.9), λ is the X-ray wavelength (0.154056 nm), B is the full-width half-maximum (in radians), and θ is the Bragg angle of the (130)/(310) peak. The XRD data clearly show that the TA treatment does not change the crystalline structure and nanoparticle size in the Sb_2S_3 film but reduces evidently the oxide defects therein.

X-ray photoelectron spectroscopic (XPS) measurements were carried out to further investigate the effect of TA treatment on the Sb_2S_3 film. As shown in Figure 1e, the XPS Sb 3d spectra of both Sb_2S_3 and Sb_2S_3(TA) films exhibit the peaks at 540 eV for the Sb−O in Sb_2O_3 and 538.9 eV for the Sb−S in Sb_2S_3,[23−25] but the S−O peak of the Sb_2S_3(TA) film is relatively much weaker (Figure 1e). Obviously, the XPS data demonstrate that the TA treatment remarkably reduces the Sb_2O_3 second phase in the Sb_2S_3 film, in agreement with the XRD data. It is well accepted that TA was decomposed into H_2S gas during the followed thermal annealing at 300 °C and reacted with Sb_2O_3 into Sb_2S_3.[23−25]

The TiO_2/CdS/$CuInS_2$ ternary planar heterojunction film prepared on FTO substrate consists of ca. 120 nm-thick TiO_2 nanoparticle layer, 60 nm-thick CdS nanoparticle layer, and 160 nm-thick $CuInS_2$ nanoparticle layer (Figure S1). After the deposition of Sb_2S_3 film, we obtain the TiO_2/CdS/$CuInS_2$/Sb_2S_3 quaternary planar heterojunction film on FTO substrate (Figure 2a), in which the superstrate structure is well distinguished and the Sb_2S_3 film of ca. 50 nm thickness exhibits a quite compact morphology. Our results showed that the Sb_2S_3 film thickness was determined by the chemical bath deposition (CBD) time for Sb_2S_3 deposition and increasing the CBD time led to a thicker Sb_2S_3 film with an increased absorbance (Figures S1 and S2). Ultraviolet photoelectron spectroscopy (UPS) was used to determine the Fermi level (E_f) and the valence band maximum (E_{VBM}) of the Sb_2S_3 and Sb_2S_3(TA) films (Figure S3). As shown in Figure 2b, the cut-off binding energy ($E_{cut\text{-}off}$) is determined by the intercept of the linear portion of the spectra (high binding energy edge) with baseline, the $E_f - E_{VBM}$ is evaluated by the intersection of the linear portion of the spectra with the baseline in the low binding energy region. With $E_f = -21.22 + E_{cut\text{-}off}$, the Sb_2S_3 and Sb_2S_3(TA) films are estimated to have the E_f of −4.79 and −4.73 eV and the E_{VBM} of −5.22 and −5.09 eV, respectively. In combination with the optical E_g of 1.77 eV, the conduction

https://dx.doi.org/10.1021/acsomega.0c06231
ACS Omega 2021, 6, 6973−6980

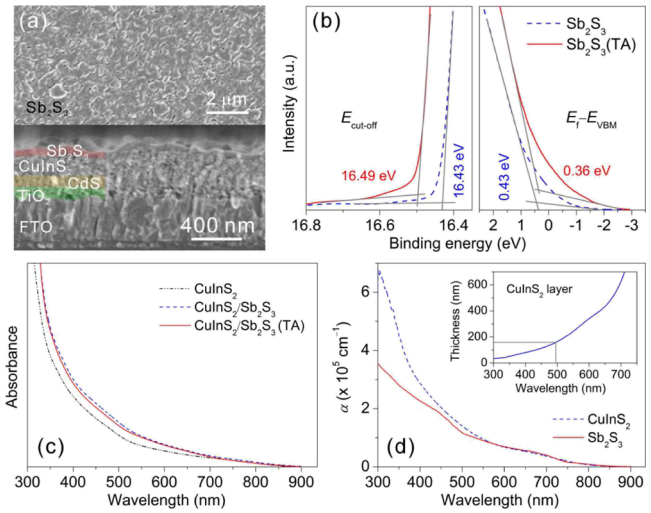

Figure 2. (a) SEM images (above: bird's eye view; below: cross-sectional view) of the Sb_2S_3 film deposited on FTO/TiO_2/CdS/$CuInS_2$ substrate. (b) UPS spectra of Sb_2S_3 and Sb_2S_3(TA) films prepared on FTO/TiO_2/CdS/$CuInS_2$ substrates. (c) Absorption spectra of $CuInS_2$, $CuInS_2/Sb_2S_3$, and $CuInS_2/Sb_2S_3$(TA) films on FTO/TiO_2/CdS substrates. (d) Absorption coefficients of the $CuInS_2$ and Sb_2S_3 films dependent on wavelength, where the $CuInS_2$ and Sb_2S_3 films were respectively deposited on FTO/TiO_2/CdS and FTO/TiO_2/CdS/$CuInS_2$ substrates, and the inset is the calculated $CuInS_2$ film thickness required to absorb 90% incident photons of a specific wavelength.

band minimum (E_{CBM}) levels of the Sb_2S_3 and Sb_2S_3(TA) films are estimated to be −3.45 and −3.32 eV, respectively.

As shown in Figure 2c, the $CuInS_2$ film exhibits a broad shoulder with a tail in the long wavelength direction due to broad size distribution of $CuInS_2$ nanoparticles.[12,26] After depositing an Sb_2S_3 or Sb_2S_3(TA) film, the resulting $CuInS_2/Sb_2S_3$ and $CuInS_2/Sb_2S_3$(TA) films exhibit almost the same absorption featuring a slightly enhanced absorption in the spectral range of <700 nm in comparison to the pure $CuInS_2$ film as a result of the Sb_2S_3 contribution. In order to determine the absorption coefficient (α) of the $CuInS_2$ and Sb_2S_3 films, their transmission spectra were measured (Figure S4). The dependence of α on wavelength was calculated using the relation $\alpha = d^{-1} \ln(T^{-1})$, where d is the thickness and T is the measured transmittance. As shown in Figure 3d, the $CuInS_2$ and Sb_2S_3 films almost have the same α in the wavelength range of 550−900 nm. Inset to Figure 2d is the $CuInS_2$ film thickness required for absorbing 90% of incident photons of a specific wavelength, showing that the 160 nm-thick $CuInS_2$ film mainly absorbs the photons below ca. 490 nm.

2.2. Solar Cell. The cross-sectional SEM image of a finished solar cell clearly shows the FTO/TiO_2/CdS/$CuInS_2$/Sb_2S_3/Au superstrate architecture (Figure 3a), in which the Sb_2S_3 film is an interfacial layer (IL) between the $CuInS_2$ photon harvester film and collection electrode. With the work-function (W_f), conduction band level (E_{CB}), and valence band level (E_{VB}) values in the literature, that is, W_f = −5.10 eV for Au and −4.40 eV for FTO,[22] E_{CB} = −4.20 eV and E_{VB} = −7.40 eV for TiO_2,[27] E_{CB} = −3.98 eV and E_{VB} = −6.38 eV for CdS,[28] and E_{CB} = −3.67 eV and E_{VB} = −5.27 eV for $CuInS_2$,[12] the band level alignments among the materials are depicted in Figure 3b. In the all-inorganic solar cell, obviously, the material components actually form the type-II heterojunctions facilitating charge transport, where the TiO_2, CdS, and $CuInS_2$ films act, respectively, as the selective transporter of photogenerated

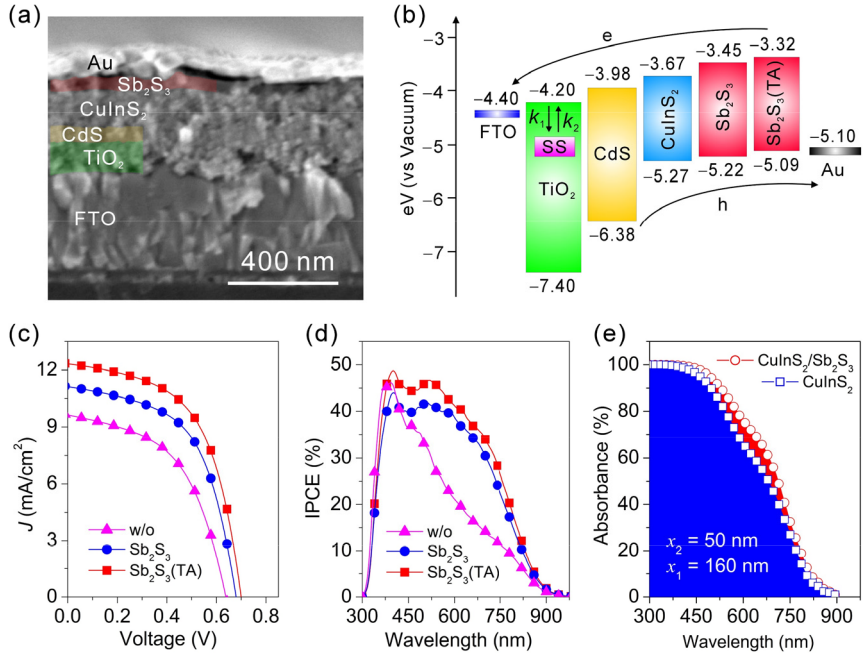

Figure 3. (a) Cross-sectional SEM image of a practical FTO/TiO_2/CdS/$CuInS_2$/Sb_2S_3/Au all-inorganic solar cell. (b) Band-level alignments and charge transfer in the all-inorganic solar cell, where the photogenerated electrons injected into the conduction band of TiO_2 may be trapped (k_1) by surface states (SS) and the trapped electrons can be thermally released (k_2) into the conduction band. (c) J−V curves and (d) IPCE spectra of the best ITO/TiO_2/CdS/$CuInS_2$/IL/Au solar cells without IL (w/o) and with Sb_2S_3 or Sb_2S_3(TA) film as IL. (e) Calculated absorbance spectra of $CuInS_2$ film and $CuInS_2/Sb_2S_3$ layer derived from the wavelength-dependent absorption coefficients of $CuInS_2$ and Sb_2S_3 films in Figure 2d, for which the $CuInS_2$ and Sb_2S_3 films are 160 nm (x_1) and 50 nm (x_2) in thickness, respectively.

https://dx.doi.org/10.1021/acsomega.0c06231
ACS Omega 2021, 6, 6973−6980

Table 1. Performance of the FTO/TiO_2/CdS/$CuInS_2$/IL/Au Solar Cells[a]

IL	V_{oc} (V)	J_{sc} (mA/cm^2)	FF (%)	η (%)	R_s (Ω·cm^2)	R_{sh} (Ω·cm^2)
w/o	0.64 ± 0.02	8.19 ± 0.80	54.17 ± 2.68	2.85 ± 0.25	18.63 ± 4.58	537.08 ± 96.74
	0.64	9.61	51.39	3.15	17.21	380.76[b]
Sb_2S_3	0.68 ± 0.00	10.85 ± 0.69	53.68 ± 1.67	3.97 ± 0.22	13.55 ± 2.28	448.43 ± 76.60
	0.68	11.09	56.04	4.22	11.22	478.52[b]
Sb_2S_3(TA)	0.69 ± 0.01	11.83 ± 0.51	55.79 ± 1.70	4.61 ± 0.14	11.59 ± 1.35	479.36 ± 70.48
	0.70	12.31	56.29	4.85	10.76	549.95[b]

[a]Each of the data with standard deviations represents the average of 10 individual devices, measured under AM 1.5G illumination (100 mW/cm^2); IL means interfacial layer; R_s and R_{sh} are the series and shunt resistances, respectively. [b]The data for the device with the best efficiency.

electrons, the interfacial spacer with ignorable absorption for the spatial separation of photogenerated charge carriers, and the photon harvester.[12] The Sb_2S_3 thickness in this experiment was adjusted by varying the CBD time for Sb_2S_3 deposition (Figures S1 and S2). Our results demonstrated that the optimal thickness of the Sb_2S_3 film for solar cells is about 50 nm obtained with the CBD time of 15 min for Sb_2S_3 deposition (Figure S5 and Table S1). On the other hand, in order to further improve the device performance, we spin-coated TA onto the Sb_2S_3 film to reduce the Sb_2O_3 therein (Figure 1d,e). The influence of TA amount on the device performance was also investigated by using different concentrations of TA solutions for spin-coating (Figure S6 and Table S2). Results showed that the peak efficiency was obtained at the TA solution concentration of 10 mg/mL. These results demonstrate that the optimal FTO/TiO_2/CdS/$CuInS_2$/Sb_2S_3/Au solar cell in this experiment features the 50 nm-thick Sb_2S_3 (CBD time: 15 min) that is treated by the TA solution of 10 mg/mL in concentration. The following discussions about the functions of the Sb_2S_3 film are mainly based on the optimized solar cells.

Figure 3c shows the current−voltage (J−V) curves of the best solar cells, and the average overall device performances for each kind of devices are summarized in Table 1. The solar cells configurated as FTO/TiO_2/CdS/$CuInS_2$/Au without IL (w/o) only achieved a power conversion efficiency (η) of 3.15% with a short-circuit current density (J_{sc}) of 9.61 mA/cm^2, an open-circuit voltage (V_{oc}) of 0.64 V, and a fill factor (FF) of 51.39%, comparable to the reported values (η = 3.0−4.0%) of similarly prepared and configurated ITO(FTO)/$CuInS_2$/CdS/Al devices,[7,8] With the pristine Sb_2S_3 film as IL, the V_{oc}, J_{sc}, and FF of the FTO/TiO_2/CdS/$CuInS_2$/Sb_2S_3/Au cells are all greatly improved, resulting in a significantly increased η up to 4.22% (Table 1). Clearly, the Sb_2S_3 film as the IL is of great importance for boosting the performance of solar cells.

The incident photon-to-current efficiency (IPCE) spectra were measured to study photocurrent generation in the solar cells (Figure 3d). The observed changes in IPCE agree with that in J_{sc} (Figure 3c and Table 1). In comparison to the FTO/TiO_2/CdS/$CuInS_2$/Au solar cell without IL (w/o), the utility of Sb_2S_3 film as IL in the FTO/TiO_2/CdS/$CuInS_2$/Sb_2S_3/Au increases the IPCE mainly within the visible range (490−850 nm). The contribution of the Sb_2S_3 film is quantitatively compared by using the integrated areas within 490−850 nm on the IPCE spectra, and the application of the Sb_2S_3 film as IL leads to a significant IPCE increase by ca. 73%. Since the $CuInS_2$ film mainly absorbs 90% of the incident photons below 490 nm (inset in Figure 2d), the Sb_2S_3 film following the $CuInS_2$ one inevitably provides complementary absorption of the photons above 490 nm. In this experiment, the retaining intensity of incident photons (I_0) after the $CuInS_2$/Sb_2S_3 layer absorption is expressed according to the relation $I(\lambda) = I_0\exp(-\alpha_{\lambda_1}x_1)\exp(-\alpha_{\lambda_2}x_2)$, where α_{λ_1} and α_{λ_2} are, respectively, the wavelength-dependent absorption coefficients of $CuInS_2$ and Sb_2S_3 films, and x_1 and x_2 are, respectively, the thicknesses of the $CuInS_2$ and Sb_2S_3 films. Using the measured absorption coefficient (α) dependent on wavelength (λ) of the $CuInS_2$ and Sb_2S_3 films (Figure 2d), the absorptance spectra of the $CuInS_2$ film and $CuInS_2$/Sb_2S_3 layer with x_1 = 160 nm and x_2 = 50 nm are calculated (Figure 3e). Clearly, the application of the Sb_2S_3 film as IL behind the $CuInS_2$ film increases the photon harvesting mainly within 490−850 nm, for which the photon absorptance is remarkably increased by ca. 15% estimated from the integrated areas on the absorptance spectra. Therefore, the absorption contribution of the Sb_2S_3 film to photocurrent generation is not negligible, but it indeed does not completely compensate for the significantly increased IPCE by 73%. While the IPCE below 490 nm reflects the absorption contribution of the whole $CuInS_2$ film (inset in Figure 2d), the IPCE in the range of 490−850 nm is also actually related to the charge carrier collection efficiency in the device.[12] Reasonably, the combinational analyses of IPCE and absorptance data indicate that the higher J_{sc} upon the application of Sb_2S_3 film as IL mainly results from the dual functions of the Sb_2S_3 film, that is, to provide the complementary absorption after $CuInS_2$ attenuation and to enhance the collection efficiency of photogenerated charge carriers.

After the Sb_2S_3 film was treated with TA to reduce the Sb_2O_3 therein (Figure 1d,e), the device J_{sc} gets further remarkably improved by 11%, but the device V_{oc} and FF are very faintly increased, resulting in a FTO/TiO_2/CdS/$CuInS_2$/Sb_2S_3(TA)/Au champion cell with an efficiency of η = 4.85% (J_{sc} = 12.31 mA/cm^2, V_{oc} = 0.70 V, and FF = 56.29%). Obviously, with reduction of the Sb_2O_3 impurity in Sb_2S_3 film by TA treatment, the IPCE within 490−850 nm gets further improved (Figure 3d), suggesting a further enhanced charge collection efficiency in that the absorption property is not altered (Figures 1c and 2c). The performance of the solar cells with the Sb_2S_3(TA) film as the IL is of higher producibility, for example, the averaged efficiency of 10 individual devices is 4.61% (Table 1). We also examined the stability of the champion device when stored at room temperature (RT) and 50 °C in N_2 atmosphere. After the storages at RT and 50 °C for 30 days, the cell still retained 94.86 and 92.78% of the initial efficiency, respectively (Figure S7). Clearly, the all-inorganic $CuInS_2$ solar cells have a good thermal stability.

For understanding the effects of the Sb_2S_3 film as IL and its TA treatment on the charge collection efficiency, the electrochemical impedance spectroscopic (EIS) spectra of solar cells were measured. The measured EIS spectra of the solar cells in the form of Nyquist plots show only one distinct

https://dx.doi.org/10.1021/acsomega.0c06231
ACS Omega 2021, 6, 6973−6980

distorted semicircle (Figure 4a), which is related to the interfacial charge recombination between electrons and

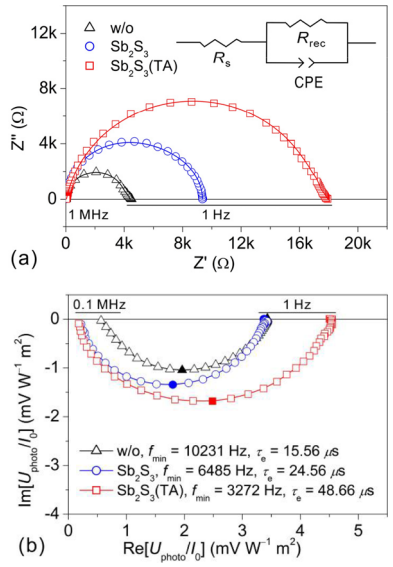

Figure 4. (a) EIS and (b) IMVS spectra of the ITO/TiO_2/CdS/$CuInS_2$/IL/Au solar cells without IL (w/o) and with Sb_2S_3 or Sb_2S_3(TA) film as IL. On plot (a), the scatters are experimental data measured in the dark, the solid lines are the fitted data, and the inset is the equivalent circuit used for fitting. The solid symbols on plot (b) identify f_{min} points.

holes.[29,30] The measured EIS spectra are fitted with an equivalent circuit based on a transmission line model,[31,32] which comprises a series resistance (R_s), a recombination resistance (R_{rec}), and constant phase-angle element (CPE) (inset in Figure 4a), and the detailed fitted parameters are summarized in Table S3. The EIS results show that, in comparison with the FTO/TiO_2/CdS/$CuInS_2$/Au solar cell without IL (R_{rec} = 385 Ω cm^2), upon the application of pristine Sb_2S_3 or Sb_2S_3(TA) film as the IL, the R_{rec} gets increased up to 834 Ω cm^2 by 117% or 1577 Ω cm^2 by 310%, respectively. Clearly, the application of Sb_2S_3 film as the IL and the further TA treatment of the Sb_2S_3 film greatly reduce the charge recombination in the solar cells, which is in good agreement with the changed shunt resistances (R_{sh}) for the leakage current due to the interfacial charge recombination and the structural defects in materials during the J−V measurements (Table 1). Moreover, with respect to the solar cells without IL, using Sb_2S_3 film or Sb_2S_3(TA) film as the IL greatly reduce the series resistance (R_s) related to the materials conductivity and the interfacial contacts from original 3.59 Ω cm^2 down to 2.95 Ω cm^2 or to 2.32 Ω cm^2 (Table S3), also in agreement with the observed R_s changes in the J−V measurements (Table 1).

In order to get insights into the changed charge recombination in the devices upon the application of the Sb_2S_3 film as the IL and its TA treatment, we used the dynamic intensity modulated photovoltage spectroscopy (IMVS) technique to study the charge recombination dynamics in the solar cells (Figure 4b). During IMVS measurements, the photovoltage (U_{ph}) response to a small sinusoidal perturbation superimposed on the background light intensity under open-circuit conditions was observed.[33] The electron lifetime (τ_e) related to the charge recombination under open-circuit condition was evaluated by the frequency (f_{min}) of the lowest imaginary component of IMVS response, according to the relation $\tau_e = (2\pi f_{min})^{-1}$. The measured IMVS spectra of the solar cells only exhibit one distorted semicircle in the fourth quadrant (positive real, negative imaginary) of the complex plane (Figure 4b), in agreement with the fact that photovoltage lags behind illumination.[34] The IMVS spectra are similar to the observations in other inorganic heterojunction solar cells.[22] The τ_e values for devices should not be the direct measures for the bulk charge recombinations inside CdS, $CuInS_2$, and/or Sb_2S_3 films because they normally occur on a timescale from picoseconds to nanoseconds.[15,35−37] Therefore, the observed time constants τ_e by IMVS reasonably correlate with the interfacial charge recombination that mainly occurs at either TiO_2/CdS or CdS/$CuInS_2$ interface. Even though the CdS absorption contribution to photocurrent generation is negligible, its photoexcitation still imposes the effects on the transport dynamics of charge carriers.[12] We have previously found in ITO/TiO_2/CdS/$CuInS_2$/Spiro-OMeTAD/Au solar cells that the τ_e (hundreds of microseconds) related to the interfacial charge recombination at the TiO_2/CdS interface is much longer than that (tens of microseconds) at the CdS/$CuInS_2$ interface.[12] Reasonably, the τ_e values (tens of microseconds) in this experiment are related to the charge recombination at the CdS/$CuInS_2$ interface.

The charge recombination depends on the probability of opposite charges meeting together for electric coupling and therefore on the charge carrier densities.[38−40] In comparison to the solar cell without IL, using the pristine Sb_2S_3 film as the IL results in a much longer τ_e, suggesting a more efficient extraction of photogenerated holes from $CuInS_2$ film into the Au collection electrode via the Sb_2S_3 film for a greatly reduced interfacial charge recombination at the CdS/$CuInS_2$ interface. After the TA treatment, the τ_e gets further increased, inferring that the removal of Sb_2O_3 impurities as the hole-trapping centers[25] in the Sb_2S_3 film by TA treatment enhances the extraction of photogenerated holes at the $CuInS_2$/Sb_2S_3 interface and the escape of the photogenerated holes away from the CdS/$CuInS_2$ interface for the reduced interfacial charge recombination thereat. The τ_e changes due to the interfacial recombination at the CdS/$CuInS_2$ interface observed by IMVS agree with the EIS (Figure 4a) and J−V (Table 1) results. Clearly, the reduced interfacial charge recombination at the CdS/$CuInS_2$ interface results from the selective extraction of photogenerated holes by the Sb_2S_3 and Sb_2S_3(TA) films as ILs, which inevitably increases the collection efficiency of photogenerated charge carriers in the device for the enhanced IPCE in the whole spectral range, in particular within 450−850 nm, and the J_{sc} of the solar cells (Figure 3c,d).

3. CONCLUSIONS

We report a solution-processed in situ growth strategy to prepare all-inorganic $CuInS_2$ planar heterojunction solar cells configurated as FTO/TiO_2/CdS/$CuInS_2$/Sb_2S_3/Au. Under the controlled in situ growth and thioacetamide treatment of the Sb_2S_3 film as an interfacial layer on a preformed TiO_2/CdS/$CuInS_2$ superstrate heterojunction film with a defined structure, the optimized solar cell, featuring the 50 nm-thick Sb_2S_3 film deposited at the CBD time of 15 min and treated by the TA solution of 10 mg/mL in concentration, achieves the power conversion efficiency of 4.85% under AM 1.5G illumination (100 mW/cm^2) and a high stability against the temperature of 50 °C.

https://dx.doi.org/10.1021/acsomega.0c06231
ACS Omega 2021, 6, 6973−6980

The Sb_2S_3 interfacial layer has an absorption coefficient that is almost the same as that of the underlying $CuInS_2$ film in the visual range. The Sb_2S_3 interfacial layer sandwiched between the $CuInS_2$ photon-harvesting film and Au electrode is of great importance for boosting the device performance, thanks to its dual functions of providing complementary absorption after $CuInS_2$ attenuation and acting as an effective HTM layer to selectively extract photogenerated holes for improving the charge collection efficiency; moreover, the thioacetamide treatment of the Sb_2S_3 interfacial layer further improves the device performance by reducing the Sb_2O_3 hole-trapping centers therein to enhance the interfacial hole extraction efficiency at the $CuInS_2/Sb_2S_3$ interface. In the long term, this work will have a significant impact on designing an effective inorganic HTM layer with a complementary absorption for efficient and stable all-inorganic solar cells.

4. EXPERIMENTAL SECTION

4.1. In Situ Growth of Sb_2S_3 Film. In order to get an easy characterization of the in situ grown Sb_2S_3 film, the deposition of Sb_2S_3 films was carried out on FTO/TiO_2 substrates that were obtained by depositing TiO_2 film on FTO substrate as described previously.[12] The Sb_2S_3 film was prepared by the CBD method as described elsewhere.[22] After being immersed in the mixture solution of $SbCl_3$ acetone solution (0.3 M) and $Na_2S_2O_3$ aqueous solution (0.3 M) at ca. 7 °C for a given time (normally 15 min, unless otherwise specified) to deposit Sb_2S_3, the FTO/TiO_2 substrate was washed with deionized water and dried at 65 °C in vacuum overnight and then thermally annealed on a hot plate at 300 °C for 5 min under N_2 atmosphere, resulting in the Sb_2S_3 film on the FTO/TiO_2 substrate. Furthermore, a certain amount of TA was spin-coated (3000 rpm, 30 s) onto the Sb_2S_3 film from the TA solutions in DMF (normally 10 mg/mL, unless otherwise specified), followed by annealing at 300 °C for 2 min in N_2 atmosphere, resulting in the Sb_2S_3(TA) film on the FTO/TiO_2 substrate.

4.2. Fabrication of the Solar Cell. FTO/TiO_2/CdS/$CuInS_2$ superstrate heterojunction was prepared by sequential in situ growth of nanostructured TiO_2 layer, nanostructured CdS layer, and nanostructured $CuInS_2$ layer on a FTO glass substrate by the method described elsewhere,[12] in which the thicknesses of TiO_2, CdS, and $CuInS_2$ layers were ca. 120, 60, and 160 nm, respectively (Figure S1). In order to fabricate the all-inorganic solar cells with a configuration of FTO/TiO_2/CdS/$CuInS_2$/IL/Au, an Sb_2S_3 or Sb_2S_3(TA) interfacial layer (IL) was in situ grown on the FTO/TiO_2/CdS/$CuInS_2$ substrate by the method same as that for its growth on the FTO/TiO_2 substrate. Finally, a Au electrode (ca. 100 nm in thickness) was deposited by thermal evaporation through a shadow mask to form an overlapped area of 3 × 3 mm^2 between FTO and Au electrode. The solar cell was encapsulated in a N_2 atmosphere. Moreover, the FTO/TiO_2/CdS/$CuInS_2$/Au solar cells without an IL layer were also fabricated for comparison.

4.3. Instruments and Characterization. The XRD patterns, SEM images, absorption spectra, XPS spectra, and UPS spectra of the film samples were obtained, the $J-V$ characteristics of solar cells were measured under AM 1.5G illumination (100 mW/cm^2), the IPCE spectra and IMVS spectra of solar cells were obtained as described elsewhere.[12] During the $J-V$ and IMVS measurements, the illumination area of each solar cell was limited by a mask with an aperture (3 × 3 mm^2) to the overlapped area between FTO and Au electrode, which actually defined the effective area for getting photovoltaic parameters of the device. The EIS spectra of the devices were measured in the dark at 0.6 V bias voltage with a frequency ranging from 1 Hz to 1 MHz on an electrochemical workstation (IM6e, Zahner Co.).

■ ASSOCIATED CONTENT

Supporting Information

The Supporting Information is available free of charge at https://pubs.acs.org/doi/10.1021/acsomega.0c06231.

Additional characterization data including SEM, UV−vis absorption, UPS data, and transmission spectra for the in situ growth of Sb_2S_3 films and additional solar cell data including the device $J-V$ performance dependent on CBD time and TA concentration, the solar cell stability, and the parameters for fitting EIS data (PDF)

■ AUTHOR INFORMATION

Corresponding Authors

Mingtai Wang − *Institute of Solid State Physics, HFIPS, Chinese Academy of Sciences, Hefei 230031, P. R. China;* orcid.org/0000-0002-5038-5020; Email: mtwang@ipp.ac.cn

Chao Dong − *Institute of Solid State Physics, HFIPS, Chinese Academy of Sciences, Hefei 230031, P. R. China;* orcid.org/0000-0002-1464-4195; Email: chaodone@126.com

Authors

Wangwei Chen − *Institute of Solid State Physics, HFIPS, Chinese Academy of Sciences, Hefei 230031, P. R. China; University of Science and Technology of China, Hefei 230026, P. R. China;* orcid.org/0000-0003-0000-8857

Wenbo Cao − *Institute of Solid State Physics, HFIPS, Chinese Academy of Sciences, Hefei 230031, P. R. China; University of Science and Technology of China, Hefei 230026, P. R. China*

Rong Liu − *Institute of Solid State Physics, HFIPS, Chinese Academy of Sciences, Hefei 230031, P. R. China; University of Science and Technology of China, Hefei 230026, P. R. China*

Zhiyang Wan − *Institute of Solid State Physics, HFIPS, Chinese Academy of Sciences, Hefei 230031, P. R. China; University of Science and Technology of China, Hefei 230026, P. R. China*

Junwei Chen − *Institute of Solid State Physics, HFIPS, Chinese Academy of Sciences, Hefei 230031, P. R. China;* orcid.org/0000-0003-0574-874X

Getinet Y. Ashebir − *Institute of Solid State Physics, HFIPS, Chinese Academy of Sciences, Hefei 230031, P. R. China; University of Science and Technology of China, Hefei 230026, P. R. China*

Complete contact information is available at: https://pubs.acs.org/10.1021/acsomega.0c06231

Notes

The authors declare no competing financial interest.

■ ACKNOWLEDGMENTS

This work was supported by the National Natural Science Foundation of China (grant nos. 11474286, 11974353), the

National Science Foundation for Young Scientists of China (grant no. 52002373), the Collaborative Innovation Program of Hefei Science Center, CAS (grant no. 2020HSC-CIP004), and the HFIPS President Foundation (grant no. YZJJZX202018).

REFERENCES

(1) Klaer, J.; Bruns, J.; Henninger, R.; Siemer, K.; Klenk, R.; Ellmer, K.; Bräunig, D. Efficient $CuInS_2$ Thin-Film Solar Cells Prepared by a Sequential Process. *Semicond. Sci. Technol.* **1998**, *13*, 1456−1458.
(2) Siemer, K.; Klaer, J.; Luck, I.; Bruns, J.; Klenk, R.; Bräunig, D. Efficient $CuInS_2$ Solar Cells from a Rapid Thermal Process (RTP). *Sol. Energy Mater. Sol. Cells* **2001**, *67*, 159−166.
(3) Scheer, R.; Klenk, R.; Klaer, J.; Luck, I. $CuInS_2$ Based Thin Film Photovoltaics. *Sol. Energy* **2004**, *77*, 777−784.
(4) Klenk, R.; Klaer, J.; Scheer, R.; Lux-Steiner, M. C.; Luck, I.; Meyer, N.; Rühle, U. Solar Cells Based on $CuInS_2$−An Overview. *Thin Solid Films* **2005**, *480-481*, 509−514.
(5) Rühle, S. Tabulated Values of the Shockley−Queisser Limit for Single Junction Solar Cells. *Sol. Energy* **2016**, *130*, 139−147.
(6) Zimmermann, E.; Pfadler, T.; Kalb, J.; Dorman, J. A.; Sommer, D.; Hahn, G.; Weickert, J.; Schmidt-Mende, L. Toward High-Efficiency Solution-Processed Planar Heterojunction Sb_2S_3 Solar Cells. *Adv. Sci.* **2015**, *2*, 1500059.
(7) Li, L.; Coates, N.; Moses, D. Solution-Processed Inorganic Solar Cell Based on in Situ Synthesis and Film Deposition of $CuInS_2$ Nanocrystals. *J. Am. Chem. Soc.* **2010**, *132*, 22−23.
(8) Azimi, H.; Heumüller, T.; Gerl, A.; Matt, G.; Kubis, P.; Distaso, M.; Ahmad, R.; Akdas, T.; Richter, M.; Peukert, W.; Brabec, C. J. Relation of Nanostructure and Recombination Dynamics in a Low-Temperature Solution-Processed $CuInS_2$ Nanocrystalline Solar Cell. *Adv. Energy Mater.* **2013**, *3*, 1589−1596.
(9) Cheshmekhavar, A. H.; Mahjoub, A. R.; Fakhri, H.; Dehghani, M. An All Solution-Based Process for the Fabrication of Superstrate-Type Configuration $CuInS_2$ Thin Film Solar Cells. *RSC Adv.* **2015**, *5*, 97381−97390.
(10) Cheshme khavar, A. H.; Mahjoub, A.; Samghabadi, F. S.; Taghavinia, N. Fabrication of Selenization-Free Superstrate-Type $CuInS_2$ Solar Cells Based on All-Spin-Coated Layers. *Mater. Chem. Phys.* **2017**, *186*, 446−455.
(11) Golobostanfard, M. R.; Abdizadeh, H.; Jannati, A. Solution Processable Wurtzite $CuInS_2$ Inverted Type Solar Cell. *Sol. Energy Mater. Sol. Cells* **2017**, *164*, 1−6.
(12) Chen, W.; Qi, J.; Dong, C.; Chen, J.; Shen, Z.; He, Y.; Yang, S.; Chen, T.; Chen, C.; Li, Y.; Li, M.-D.; Wang, M. Solution-Processed in Situ Growth of $CuInS_2$ Nanoparticle Films for Efficient Planar Heterojunction Solar Cells with a Dual Nature of Charge Generation. *ACS Appl. Energy Mater.* **2019**, *2*, 5231−5242.
(13) You, J.; Meng, L.; Song, T.-B.; Guo, T.-F.; Yang, Y.; Chang, W.-H.; Hong, Z.; Chen, H.; Zhou, H.; Chen, Q.; Liu, Y.; De Marco, N.; Yang, Y. Improved Air Stability of Perovskite Solar Cells via Solution-Processed Metal Oxide Transport Layers. *Nat. Nanotechnol.* **2016**, *11*, 75−81.
(14) Jin, X.; Yuan, Y.; Jiang, C.; Ju, H.; Jiang, G.; Liu, W.; Zhu, C.; Chen, T. Solution Processed NiO_x Hole-Transporting Material for All-Inorganic Planar Heterojunction Sb_2S_3 Solar Cells. *Sol. Energy Mater. Sol. Cell.* **2018**, *185*, 542−548.
(15) Christians, J. A.; Leighton, D. T., Jr.; Kamat, P. V. Rate Limiting Interfacial Hole Transfer in Sb_2S_3 Solid-State Solar Cells. *Energy Environ. Sci.* **2014**, *7*, 1148−1158.
(16) Huerta-Flores, A. M.; García-Gómez, N. A.; De la Parra-Arciniega, S. M.; Sánchez, E. M. Fabrication and Characterization of a Nanostructured TiO_2/In_2S_3-Sb_2S_3/CuSCN Extremely Thin Absorber (eta) Solar Cell. *Semicond. Sci. Technol.* **2016**, *31*, 085011.
(17) Arora, N.; Dar, M. I.; Hinderhofer, A.; Pellet, N.; Schreiber, F.; Zakeeruddin, S. M.; Grätzel, M. Perovskite Solar Cells with CuSCN Hole Extraction Layers Yield Stabilized Efficiencies Greater Than 20%. *Science* **2017**, *358*, 768−771.
(18) Sun, W.; Li, Y.; Ye, S.; Rao, H.; Yan, W.; Peng, H.; Li, Y.; Liu, Z.; Wang, S.; Chen, Z.; Xiao, L.; Bian, Z.; Huang, C. High-Performance Inverted Planar Heterojunction Perovskite Solar Cells Based on a Solution Processed CuO_x Hole Transport Layer. *Nanoscale* **2016**, *8*, 10806−10813.
(19) Yu, Z.; Liu, W.; Fu, W.; Zhang, Z.; Yang, W.; Wang, S.; Li, H.; Xu, M.; Chen, H. An Aqueous Solution-Processed CuO_x Film as an Anode Buffer Layer for Efficient and Stable Organic Solar Cells. *J. Mater. Chem. A* **2016**, *4*, 5130−5136.
(20) Kondrotas, R.; Chen, C.; Tang, J. Sb_2S_3 Solar Cells. *Joule* **2018**, *2*, 857−878.
(21) Lei, H.; Chen, J.; Tan, Z.; Fang, G. Review of Recent Progress in Antimony Chalcogenide-Based Solar Cells: Materials and Devices. *Sol. RRL* **2019**, *3*, 1900026.
(22) Qiu, Z.; Liu, C.; Pan, G.; Meng, W.; Yue, W.; Chen, J.; Zhou, X.; Zhang, F.; Wang, M. Solution-Processed Solar Cells Based on Inorganic Bulk Heterojunctions with Evident Hole Contribution to Photocurrent Generation. *Phys. Chem. Chem. Phys.* **2015**, *17*, 12328−12339.
(23) Ye, Q.; Xu, Y.; Chen, W.; Yang, S.; Zhu, J.; Weng, J. Enhanced Photovoltaic Performance of Sb_2S_3-Sensitized Solar Cells through Surface Treatments. *Appl. Surf. Sci.* **2018**, *440*, 294−299.
(24) Qi, J.; Dong, C.; Ashebir, G. Y.; Wan, Z.; Chen, W.; Zhao, Q.; Wang, M. Effects of Annealing Atmosphere on Composition, Structure and Photovoltaic Properties of Solution-Processed Sb_2S_3 Thin Films. *Chem. J. Chin. Univ.* **2019**, *2*, 342−349.
(25) Choi, Y. C.; Lee, D. U.; Noh, J. H.; Kim, E. K.; Seok, S. I. Highly Improved Sb_2S_3 Sensitized-Inorganic−Organic Heterojunction Solar Cells and Quantification of Traps by Deep-Level Transient Spectroscopy. *Adv. Funct. Mater.* **2014**, *24*, 3587−3592.
(26) Zhong, H.; Lo, S. S.; Mirkovic, T.; Li, Y.; Ding, Y.; Li, Y.; Scholes, G. D. Noninjection Gram-Scale Synthesis of Monodisperse Pyramidal $CuInS_2$ Nanocrystals and Their Size-Dependent Properties. *ACS Nano* **2010**, *4*, 5253−5262.
(27) Zhang, Y.; Li, J.; Jiang, G.; Liu, W.; Yang, S.; Zhu, C.; Chen, T. Selenium-Graded $Sb_2(S_{1-x}Se_x)_3$ for Planar Heterojunction Solar Cell Delivering a Certified Power Conversion Efficiency of 5.71%. *Sol. RRL* **2017**, *1*, 1700017.
(28) Xu, Y.; Schoonen, M. A. A. The Absolute Energy Positions of Conduction and Valence Bands of Selected Semiconducting Minerals. *Am. Mineral.* **2000**, *85*, 543−556.
(29) Dong, H. P.; Li, Y.; Wang, S. F.; Li, W. Z.; Li, N.; Guo, X. D.; Wang, L. D. Interface Engineering of Perovskite Solar Cells with PEO for Improved Performance. *J. Mater. Chem. A* **2015**, *3*, 9999−10004.
(30) Abdulrahim, S. M.; Ahmad, Z.; Bahadra, J.; Al-Thani, N. J. Electrochemical Impedance Spectroscopy Analysis of Hole Transporting Material Free Mesoporous and Planar Perovskite Solar Cells. *Nanomaterials* **2020**, *10*, 1635.
(31) Zhou, P.; Fang, Z.; Zhou, W.; Qiao, Q.; Wang, M.; Chen, T.; Yang, S. Nonconjugated Polymer Poly(vinylpyrrolidone) as an Efficient Interlayer Promoting Electron Transport for Perovskite Solar Cells. *ACS Appl. Mater. Interfaces* **2017**, *9*, 32957−32964.
(32) Zhang, L.; Jiang, C.; Wu, C.; Ju, H.; Jiang, G.; Liu, W.; Zhu, C.; Chen, T. V_2O_5 as Hole Transporting Material for Efficient All Inorganic Sb_2S_3 Solar Cells. *ACS Appl. Mater. Interfaces* **2018**, *10*, 27098−27105.
(33) Qi, J.; Chen, J.; Meng, W.; Wu, X.; Liu, C.; Yue, W.; Wang, M. Recent Advances in Hybrid Solar Cells Based on Metal Oxide Nanostructures. *Synth. Met.* **2016**, *222*, 42−65.
(34) Krüger, J.; Plass, R.; Grätzel, M.; Cameron, P. J.; Peter, L. M. Charge Transport and Back Reaction in Solid-State Dye-Sensitized Solar Cells: A Study Using Intensity-Modulated Photovoltage and Photocurrent Spectroscopy. *J. Phys. Chem. B* **2003**, *107*, 7536−7539.
(35) Hu, W.; Ludwig, J.; Pattengale, B.; Yang, S.; Liu, C.; Zuo, X.; Zhang, X.; Huang, J. Unravelling the Correlation of Electronic Structure and Carrier Dynamics in $CuInS_2$ Nanoparticles. *J. Phys. Chem. C* **2018**, *122*, 974−980.
(36) Grennell, A. N.; Utterback, J. K.; Pearce, O. M.; Wilker, M. B.; Dukovic, G. Relationships between Exciton Dissociation and Slow

https://dx.doi.org/10.1021/acsomega.0c06231
ACS Omega 2021, 6, 6973−6980

Recombination within ZnSe/CdS and CdSe/CdS Dot-in-Rod Heterostructures. *Nano Lett.* **2017**, *17*, 3764−3774.
(37) Christians, J. A.; Kamat, P. V. Trap and Transfer. Two-Step Hole Injection Across the Sb_2S_3/CuSCN Interfacein Solid-State Solar Cells. *ACS Nano* **2013**, *7*, 7967−7974.
(38) Lakhwani, G.; Rao, A.; Friend, R. H. Bimolecular Recombination in Organic Photovoltaics. *Annu. Rev. Phys. Chem.* **2014**, *65*, 557−581.
(39) Heiber, M. C.; Nguyen, T.-Q.; Deibel, C. Charge Carrier Concentration Dependence of Encounter-Limited Bimolecular Recombination in Phase-Separated Organic Semiconductor Blends. *Phys. Rev. B* **2016**, *93*, 205204.
(40) Engmann, S.; Ro, H. W.; Herzing, A. A.; DeLongchamp, D. M.; Snyder, C. R.; Richter, L. J.; Barito, A.; Gundlach, D. J. Reduced Bimolecular Recombination in Blade-Coated, High-Efficiency, Small-Molecule Solar Cells. *J. Mater. Chem. A* **2017**, *5*, 6893−6904.

https://dx.doi.org/10.1021/acsomega.0c06231
ACS Omega 2021, 6, 6973−6980